A Proactive Controller for Human-Driven Robots based on Force/Motion Observer Mechanisms

Yanan Li, *Senior Member, IEEE*, Lin Yang, Deqing Huang, *Senior Member, IEEE*, Chenguang Yang, *Senior Member, IEEE*, and Jingkang Xia

***Abstract*—This paper investigates human-driven robots via physical interaction, which is enhanced by integrating the human partner's motion intention. A human motor control model is employed to estimate the human partner's motion intention. A system observer is developed to estimate the human's control input in this model, so that force sensing is not required. A robot controller is developed to incorporate the estimated human's motion intention, which makes the robot proactively follow the human partner's movements. Simulations and experiments on a physical robot are carried out to demonstrate the properties of our proposed controller.**

I. Introduction

Human-robot interaction (HRI) has become a popular topic in the past decades [1], [2], [3], [4]. Among various HRI systems, human-driven robots are a class of systems where the robots are guided by their human partner through a certain interface. How to design a controller for these robots remains an open problem.

On the one hand, due to highly nonlinear and uncertain dynamics of a human, it is generally challenging to study the stability and performance of a HRI system. In [5], a state-independent stability constraint was proposed for variable impedance control which is an important control strategy in HRI. In [6], a method was proposed to detect the robot's unstable behaviors and adjust the robot's impedance control gains to guarantee the system stability.

On the other hand, it is useful for a robot to understand its human partner's motion intention for an efficient interaction. Although arguably forcing humans to adapt to robots may be equally and even more effective in a certain scenario, there are lots of examples where the task performance can be improved with robots adapting to humans [7], [8], [9], [10], [11]. Human's motion intention can be estimated or recognized via speech [12], gestures [13] or haptic feedback [14]. When focusing on physical human-robot interaction, it can be achieved using the information of interaction force and motion. By assuming that a human's trajectory should follow a certain criterion, some existing works adopt the results in the field of human motor control. For example, in [15], human motion was estimated by using a minimum jerk model where nonlinear least-squares technique was used to estimate the parameters of this model. This approach was based on the kinematic information so it was not robust in the sense of a dynamic interaction. Another approach was through learning of human's dynamic model or pattern to predict human's motion, such as [16], but it required sufficient training data. A natural choice to estimate human's motion intention is to use haptic information, such as interaction force. In [17], the authors argued that the human partner's motion intention was achieved when the interaction force between the human and the robot became zero. The interaction force was also considered as a measure of the human partner's motion intention in [18], where its differentiation was used. [19] describes a cascade-loop pHRI controller, where two neural networks (NNs) in the "outer-loop" predict human motion intent and estimate a reference trajectory for the robot that the "inner-loop" controller follows. This controller also relies on human force and pose measurements. However, it is well-known that the force measurement can be noisy and many commercialized robots are still position-control-based, despite a trend to equip collaborative robots with force sensors to make them safe and legally accepted in close vicinity to humans [20]. How to estimate human's motion intention without using force sensing? In [21], a novel idea of using the change in the robot's control effort to estimate human's motion intention was proposed, which did not require force sensing but was subjected to a delay due to a passive impedance control phase.

Based on the above discussions, in this work we propose an approach to estimate the human partner's motion intention without force sensors, and rigorously analyze the system stability. For convenience of analysis, we focus on a typical HRI system: human-driven robots [22]. In this system, a human and a robot have a common target position to reach, while the target position is only known to the human but not to the robot. One may argue that this task can be accomplished by using traditional impedance control [23] with zero stiffness. However, under impedance control the robot behaves like a passive mass-damper system, which means that certain control effort has to be made by the human partner to compensate for both the robot's dynamics and the object's. To address this issue, one natural idea is to make the robot proactively move the object to the target position, so that the human's control effort is reduced. It then raises a problem for the robot about how to obtain the knowledge of the target position, i.e., the

*The work was partially supported by the National Natural Science Foundation of China under Grants U1934221 and U21A20169, the Sichuan Science and Technology Program under Grants 2021JDJQ0012 and 2020YFQ0057, the Royal Society grant IES\R3\193136 and the UK EPSRC grant EP/T006951/1.

Y. Li is with the Department of Engineering and Design, University of Sussex, Brighton BN1 9RH, UK. (email: yl557@sussex.ac.uk).

L. Yang, D. Huang and J. Xia are with the School of Electrical Engineering, Southwest Jiaotong University, Chengdu 610031, P. R. China. (email: {yanglin0,elehd,xia-jingkang}@swjtu.edu.cn).

C. Yang is with Bristol Robotics Laboratory, University of the West of England, Bristol BS16 1QY, UK. (email: cyang@ieee.org).

human partner's motion intention. The current work addresses this problem by employing a human motor control model, which indicates that if the human's control input becomes zero, then the actual position has achieved the intended target position. As the human control input is unknown to the robot, a system observer is further developed. Then, a robot controller is proposed by integrating the estimated human partner's motion intention as the robot's reference trajectory. As two estimation processes are involved, i.e., estimation of the human control input and estimation of the human partner's motion intention, how they influence each other is studied. It is rigorously demonstrated that the human partner's motion intention is estimated and the target position is reached with the help of the robot. Simulations and experiments on a Baxter robot are carried out to testify the validity and performance of our proposed method. Some preliminary results were presented in [24], without consideration of uncertainties of the human partner's dynamics and with only simulation results. Moreover, a comparison with sensorless force control and impedance control is presented to highlight the features of our proposed method.

The rest of this paper is organized in the following order: problem formulation is discussed in Section II, including introduction of the system dynamics and assumptions; the details of our proposed method and analysis of the system performance are explained in Section III; simulation and experimental results are presented in Sections IV and V, respectively; and finally conclusions are drawn in Section VI and possible future works are suggested.

II. System description

A. Dynamic model

In this work, we consider an HRI system where a human hand and a rigid robot manipulate an object and there is no relative motion between the human hand, object and robot. The object is considered as an extension of the robot, so the system dynamics in the Cartesian space are described as

$$M_x\ddot{x}+C_x\dot{x}+G_x=u+u_h \tag{1}$$

where x is the system position. u and u_h are the control inputs of the robot and human for the system, respectively. M_x stands for the inertia/mass matrix, C_x the Coriolis and centrifugal matrix and G_x the gravitational force vector. These dynamic parameters have included both the robot and object. The dynamics model in Eq. (1) has several fundamental properties that can be exploited to facilitate controller design and stability analysis [25]. In particular, the following properties will be used in later Lyapunov-theory-based stability analysis.

Property 1: The inertia/mass matrix $M_x(q)$ is a symmetric positive definite matrix.

Property 2: The matrix $2C_x(q,\dot{q})-\dot{M}_x(q)$ is a skew-symmetric matrix.

Property 3: $M_x,\ C_x,\ G_x$ are linear in terms of a suitably selected set of the physical parameters, i.e.,

$$M_x\ddot{x}+C_x\dot{x}+G_x=Y(\ddot{x},\dot{x},x)\theta$$

where $\theta\in\mathbb{R}^{n_\theta}$ is a vector of the physical parameters of the system, n_θ a positive integer denoting the number of these parameters and $Y(\ddot{x},\dot{x},x)\in\mathbb{R}^{n\times n_\theta}$ is the regression matrix which is independent of the physical parameters. Based on Property 3, the physical parameters θ can be estimated, then $M_x,\ C_x,\ G_x$ can be used in the controller design.

In a general case, the human and the robot have their own target positions to reach while these two target positions are not necessarily the same, and either of them knows only own target position but not the partner's. From the robot's point of view, if $u_h=0$, i.e. there is no interaction with the human, this problem degrades to a traditional trajectory tracking problem (when the reference is a continuous trajectory) or position regulation problem (when the reference is a position point). From the human's point of view, if $u=0$, it becomes a human motor control problem which has been investigated in the field of motor control [26]. If u and u_h are nonzero, they will both affect the system dynamics. When the partner's control input is unknown, it becomes a challenging task to design own control input. In this paper, we aim to address this issue by analyzing the traditional human motor control and robotic tracking control, and then develop a new robot controller to deal with the interaction with its human partner.

B. Human controller

For development of the robot controller and stability analysis, we need to consider the explicit form of the human controller, which is given below according to [27]:

$$u_h=-K_{hp}(x-x_h)-K_{hd}\dot{x}-\Delta \tag{2}$$

where K_{hp} is the proportional (P) controller gain, K_{hd} is the derivative (D) controller gain, x_h is the human's target position, defined as the human motion intention, and Δ represents the uncertainty in the human controller that may be due to incomplete modelling or unintentional behaviours [28], [17]. To facilitate the robot controller design, we make the following assumptions about the uncertainty component Δ:

Assumption 1: When the human input to the system becomes zero, i.e. $u_h=0$, $\Delta=0$, indicating that there is no interaction between human and robot or that the human's position target is reached, i.e. $x=x_h$.

Assumption 2: According to [29], [30] human control gains (corresponding to the Cartesian impedance parameters, i.e. stiffness and viscosity/damping) are time-varying and functions of the position. In Eq. (2), we denote the nominal part of the gains as K_{hp} and K_{hd} and lump the time-varying and uncertain part in Δ, which is thus a function of position and velocity i.e. $\Delta\equiv\Delta(x,\dot{x})$.

Assumption 1 is reasonable as the uncertainty disappears when the human input becomes zero. Assumption 2 is made considering that the uncertainty in the human controller is correlated with the system state, i.e. position x and velocity $\dot{x}$.

Based on Assumption 2, $\Delta(x,\dot{x})$ can be obtained using approaches of function approximation, such as neural networks, polynomials etc. with corresponding basis functions [31]. Among them, we choose radial basis function neural network (RBFNN), which has been used in many applications of function approximation [32]. Using RBFNN, Δ can be approximated as

$$\Delta=W_h\phi(Z)+\varepsilon \tag{3}$$

where $Z = [x^T,\ \dot{x}^T]^T \in \Omega \subset R^p$ is the NN input, $W_h \in R^{n\times l}$ is the unknown ideal weight and $l \geq 1$ is the number of the NN nodes. ε is the NN approximation error and $\phi(Z) = [\phi_1(Z), \phi_2(Z), ..., \phi_l(Z)]^T$ is the basis function, which can be a Gaussian function

$$\phi_i(Z) = \exp\Big[\frac{-(Z-\mu_i)^T(Z-\mu_i)}{\eta_i^2}\Big] \tag{4}$$

with $i = 1, 2, ..., l$, $\mu_i = [\mu_{i1}, \mu_{i2}, ..., \mu_{ip}]^T$ the center of the basis function and η_i the width. RBFNN has been proved to be able to approximate a continuous function over a compact set $\Omega_Z \subset R^p$ to an arbitrary accuracy [33], i.e. $\|\varepsilon\| \leq \varepsilon_B$ and ε_B can be arbitrarily small if l is chosen to be large enough.

Considering that K_{hp} and K_{hd} in Eq. (2) are positive definite, we notice that the human motor control model indicates the human's control objective to reach the target position x_h, subject to the uncertainty Δ. For the analysis feasibility, the human controller (2) is rewritten as

$$u_h = -f_h - K_{hp}x - K_{hd}\dot{x} - \Delta \tag{5}$$

where $f_h \equiv -K_{hp}x_h$. Note that the human controller u_h is unknown to the robot, including unknown controller gains K_{hp}, K_{hd}, motion intention x_h (thus f_h) and uncertainty component Δ.

Assumption 3: The human controller gains K_{hp} and K_{hd} and his/her target position x_h are constants, and thus f_h is a constant.

Remark 1: Unknown parameters in the human controller are assumed to be constants for the purpose of estimation. In practice, Assumption 3 may be invalid when the human needs to track a target trajectory rather than reaching a target position. Using the zero-order hold and piecewise constant function in [34], [35], a continuous trajectory can be approximated by a piecewise trajectory composed of constant target positions, and simulations and experiments will show that the proposed method still works.

C. Robot controller

The proposed robot controller u includes two components:

$$u = u_{ff} + u_{fb} \tag{6}$$

where u_{ff} is the feedforward component and u_{fb} the feedback component. Using u_{ff} to compensate for the system dynamics, we design

$$u_{ff} = M_x\ddot{x}_r + C_x\dot{x}_r + G_x \tag{7}$$

where x_r is the reference trajectory of the robot. M_x, C_x and G_x are system matrices that can be obtained by identification, as explained in Section II.A. u_{fb} is the feedback component, i.e.

$$u_{fb} = -K_p e - K_d\dot{e} \tag{8}$$

where K_p and K_d are respectively the robot's PD control gains and $e = x - x_r$ is the robot's trajectory tracking error.

D. Problem statement

By comparing (2) and (6), we see that the human and robot have their respective targets x_h and x_r so there will be a conflict if these targets are different. As a result, both the human and robot will unnecessarily make effort to compete with each other and the final position that is to be reached will be a trade-off of the human's and robot's target positions. Therefore, we propose an approach in this paper to resolve this issue.

To understand the problem under study, we firstly consider an ideal case with two additional conditions, as presented in the following theorem.

Theorem 1: If we consider the system dynamics in (1), human's and robot's respective controllers (2) and (6), with the following strict conditions satisfied:

- $x_r = x_h$ which indicates that the robot's reference trajectory is identical to the human partner's target position;
- $\Delta = 0$, i.e., there is no uncertainty in the human controller.

then the system position will eventually converge to the human partner's target position, i.e. $\lim_{t\to\infty} x = x_h$.

The proof of Theorem 1 is given in Appendix VI-A.

From Theorem 1, we can see that $\lim_{t\to\infty} x = x_h$ can be achieved if the human's target position x_h is known by the robot and there is no uncertainty in the human controller. However, the robot cannot know x_h *a priori*, which is a result of motion planning of the human's central nervous system [36]. Therefore, *the first objective of this work is to estimate unknown human target position* x_h. For this purpose, we adopt the following idea originally developed in [17]: according to Assumption 2, the human control input $u_h = 0$ yeilds $x = x_h$, so we can use u_h to observe the difference between x and x_h. However, here the human's control input u_h is unknown to the robot and is subject to the uncertainty Δ, so *the second objective is to estimate* u_h *by developing a system observer.* Compared to the existing works that are based on a movement model of which the parameters need to be estimated [15], our method uses the haptic information (estimated interaction force) to infer human movement intent without requirement of the movement model (note that the human dynamics model in this paper is for analysis purpose but not used in the controller design).

In the next section, we will detail how to achieve these objectives by developing a robot controller and prove that they can be achieved simultaneously despite their coupling effects.

III. Robot controller

This section dedicates to design of the robot controller: in the first subsection, human controller u_h is estimated by developing a system observer; then in the second subsection, the estimated human controller is used to update the robot's reference trajectory x_r, so that x_r tracks the human's target position x_h. With the robot controller (6), it will be shown that the robot's actual position x eventually reaches the human's target position x_h.

A. Observer

By substituting the robot's controller (6) into the system dynamics model in Eq. (1), we can obtain the following error dynamics:

$$M_x\ddot{e} + (C_x + K_d)\dot{e} + K_p e = u_h \tag{9}$$

For the system observer design, the above error dynamics equation is rewritten in the state-space form:

$$\begin{aligned} &\dot{\xi} = A\xi + Bu_h \\ &\xi \equiv \begin{bmatrix} e \\ \dot{e} \end{bmatrix}, A \equiv \begin{bmatrix} \mathbf{0}_n & \mathbf{I}_n \\ -M_x^{-1}K_p & -M_x^{-1}(C_x+K_d) \end{bmatrix}, \\ &B \equiv \begin{bmatrix} \mathbf{0}_n \\ M_x^{-1} \end{bmatrix}, \end{aligned} \tag{10}$$

where ξ is the system state, $\mathbf{0}_n$ a $n-$dimentional zero matrix and $\mathbf{I}_n$ a $n-$dimentional unit matrix. Since u_h in (10) is unknown, a system observer is designed as below:

$$\dot{\hat{\xi}} = A\hat{\xi} + B\hat{u}_h - L(\hat{\xi} - \xi) \tag{11}$$

where $\hat{\xi}$ stands for the estimate of the system state ξ, $\hat{u}_h$ the estimate of the human control input u_h and $L > 0$ that can be chosen by the designer. According to the human control input u_h in Eq. (5), its estimate $\hat{u}_h$ can be expanded as

$$\hat{u}_h = -\hat{f}_h - \hat{K}_{hp}x - \hat{K}_{hd}\dot{x} - \hat{W}_h\phi(x,\dot{x}) \tag{12}$$

where $\hat{f}_h$, $\hat{K}_{hp}$, $\hat{K}_{hd}$ and $\hat{W}_h$ are estimates of f_h, K_{hp}, K_{hd} and W_h, respectively.

Deducting both sides of Eq. (11) by that of Eq. (10), we have the observer's error dynamics

$$\dot{\tilde{\xi}} = A\tilde{\xi} + B\tilde{u}_h - L\tilde{\xi} \tag{13}$$

where $\tilde{\xi} = \hat{\xi} - \xi$ stands for the state estimation error, and

$$\begin{aligned} \tilde{u}_h &= \hat{u}_h - u_h, \\ \tilde{f}_h &= \hat{f}_h - f_h,\ \tilde{K}_{hp} = \hat{K}_{hp} - K_{hp}, \\ \tilde{K}_{hd} &= \hat{K}_{hd} - K_{hd},\ \tilde{W}_h = \hat{W}_h - W_h \end{aligned} \tag{14}$$

Therefore, the estimation error of the human controller

$$\tilde{u}_h = -\tilde{f}_h - \tilde{K}_{hp}x - \tilde{K}_{hd}\dot{x} - \tilde{W}_h\phi(x,\dot{x}) + \varepsilon \tag{15}$$

B. Update laws

In this subsection, we will develop update laws to obtain the estimated parameters in Eq. (12). For this purpose, let us consider a Lyapunov function candidate as below

$$\begin{aligned} V &= V_1 + V_2 + V_3 \\ V_1 &= \frac{1}{2}(\dot{e}^T M_x \dot{e} + e^T K_p e) \\ V_2 &= \frac{1}{2}((\tilde{\xi}^T\tilde{\xi} + \tilde{f}_h^T\tilde{f}_h + \mathrm{vec}^T(\tilde{K}_{hp})\mathrm{vec}(\tilde{K}_{hp})) \\ &\quad + \mathrm{vec}^T(\tilde{K}_{hd})\mathrm{vec}(\tilde{K}_{hd})) + \mathrm{vec}^T(\tilde{W}_h)\mathrm{vec}(\tilde{W}_h))) \\ V_3 &= \frac{1}{2}(x - x_h)^T K_{hp}(x - x_h) \end{aligned} \tag{16}$$

where $\mathrm{vec}(\cdot)$ stands for the vectorisation of a matrix. Taking the time derivative of V_1, it yields

$$\dot{V}_1 = \dot{e}^T(M_x\ddot{e} + \frac{1}{2}\dot{M}_x\dot{e}) + \dot{e}^T K_p e \tag{17}$$

Considering Property 2 and the error dynamics (9), the above equation can be further written as

$$\begin{aligned} \dot{V}_1 &= \dot{e}^T(M_x\ddot{e} + C_x\dot{e} + K_p e) \\ &= \dot{e}^T(-K_d\dot{e} + u_h) = -\dot{e}^T K_d\dot{e} + \dot{e}^T u_h \end{aligned} \tag{18}$$

Taking the time derivative of V_2, it yields

$$\begin{aligned} \dot{V}_2 &= \tilde{\xi}^T\dot{\tilde{\xi}} + \tilde{f}_h^T\dot{\tilde{f}}_h + \mathrm{vec}^T(\tilde{K}_{hp})\mathrm{vec}(\dot{\tilde{K}}_{hp}) \\ &\quad + \mathrm{vec}^T(\tilde{K}_{hd})\mathrm{vec}(\dot{\tilde{K}}_{hd}) + \mathrm{vec}^T(\tilde{W}_h)\mathrm{vec}(\dot{\tilde{W}}_h) \\ &= \tilde{\xi}^T\dot{\tilde{\xi}} + \tilde{f}_h^T\dot{\tilde{f}}_h + \mathrm{vec}^T(\tilde{K}_{hp})\mathrm{vec}(\dot{\hat{K}}_{hp}) \\ &\quad + \mathrm{vec}^T(\tilde{K}_{hd})\mathrm{vec}(\dot{\hat{K}}_{hd}) + \mathrm{vec}^T(\tilde{W}_h)\mathrm{vec}(\dot{\hat{W}}_h) \end{aligned} \tag{19}$$

where $\dot{f}_h = 0$, $\dot{K}_{hp} = 0$, $\dot{K}_{hd} = 0$ and $\dot{W}_h = 0$ on the basis of Assumption 3 have been used.

Considering the estimation error of the human controller in Eq. (15), we design the update laws as below:

$$\begin{aligned} &\dot{\hat{f}}_h = B^T\tilde{\xi} + \alpha\hat{u}_h,\ \dot{\hat{K}}_{hp} = (B^T\tilde{\xi} + \alpha\hat{u}_h)x^T, \\ &\dot{\hat{K}}_{hd} = (B^T\tilde{\xi} + \alpha\hat{u}_h)\dot{x}^T,\ \dot{\hat{W}}_h = (B^T\tilde{\xi} + \alpha\hat{u}_h)\phi^T \end{aligned} \tag{20}$$

where $\alpha > 0$ is the update rate. It can be increased to speed up the update process but a too large value of α will lead to overshoot and even instability. By substituting the above update laws into $\dot{V}_2$, we can obtain

$$\begin{aligned} \dot{V}_2 &= \tilde{\xi}^T((A-L)\tilde{\xi} + B\tilde{u}_h) + \tilde{f}_h^T(B^T\tilde{\xi} + \alpha\hat{u}_h) \\ &\quad + \mathrm{vec}^T(\tilde{K}_{hp})\mathrm{vec}((B^T\tilde{\xi} + \alpha\hat{u}_h)x^T)) \\ &\quad + \mathrm{vec}^T(\tilde{K}_{hd})\mathrm{vec}((B^T\tilde{\xi} + \alpha\hat{u}_h)\dot{x}^T)) \\ &\quad + \mathrm{vec}^T(\tilde{W}_h)\mathrm{vec}((B^T\tilde{\xi} + \alpha\hat{u}_h)\phi^T)) \\ &= \tilde{\xi}^T(A-L)\tilde{\xi} + \tilde{\xi}^T B\tilde{u}_h - (\tilde{u}_h - \varepsilon)^T B^T\tilde{\xi} \\ &\quad - \alpha(\tilde{u}_h - \varepsilon)^T\hat{u}_h \\ &= \tilde{\xi}^T(A-L)\tilde{\xi} - \alpha\tilde{u}_h^T\hat{u}_h + \varepsilon^T B^T\tilde{\xi} + \alpha\varepsilon^T\hat{u}_h \end{aligned} \tag{21}$$

Taking the time derivative of V_3, we can obtain

$$\begin{aligned} \dot{V}_3 &= \dot{x}^T K_{hp}(x - x_h) \\ &= \dot{x}^T(-u_h - K_{hd}\dot{x} - W_h\phi - \varepsilon) \\ &= -\dot{x}^T u_h - \dot{x}^T K_{hd}\dot{x} - \dot{x}^T W_h\phi - \dot{x}^T\varepsilon \end{aligned} \tag{22}$$

where $\dot{x}_h = 0$ on the basis of Assumption 3 has been used.

With the estimated human controller, the robot's reference trajectory x_r can be updated to minimize it, i.e.

$$\dot{x}_r = \alpha\hat{u}_h \tag{23}$$

Then, by combining Eqs. (18) and (22), we have

$$\begin{aligned} &\dot{V}_1 + \dot{V}_3 \\ &= -\dot{e}^T K_d\dot{e} - \dot{x}_r^T u_h - \dot{x}^T K_{hd}\dot{x} - \dot{x}^T W_h\phi - \dot{x}^T\varepsilon \\ &= -\dot{e}^T K_d\dot{e} - \alpha\hat{u}_h^T u_h - \dot{x}^T K_{hd}\dot{x} - \dot{x}^T W_h\phi - \dot{x}^T\varepsilon \\ &= -\dot{e}^T K_d\dot{e} - \alpha\hat{u}_h^T\hat{u}_h + \alpha\hat{u}_h^T\tilde{u}_h - \dot{x}^T K_{hd}\dot{x} - \dot{x}^T W_h\phi \\ &\quad - \dot{x}^T\varepsilon \end{aligned} \tag{24}$$

By further combining Eqs. (21) and (24), we obtain

$$\begin{aligned} \dot{V} &= -\dot{e}^T K_d\dot{e} - \tilde{\xi}^T(L-A)\tilde{\xi} - \alpha\hat{u}_h^T\hat{u}_h - \dot{x}^T K_{hd}\dot{x} \\ &\quad - \dot{x}^T W_h\phi - \dot{x}^T\varepsilon + \varepsilon^T B^T\tilde{\xi} + \alpha\varepsilon^T\hat{u}_h \end{aligned} \tag{25}$$

Eq. (25) shows the time derivative of V, thus indicating how the Lyapunov function V changes. In the following, we need to discuss two cases to establish the system stability.

In **Case 1**: $\dot{V} < 0$ indicates that V moronically decreases with respect to time. Since $V \geq 0$, we can obtain that $\lim_{t\to\infty} V = 0$. According to the definition of V, we further obtain $\lim_{t\to\infty} \dot{e} = 0$, $\lim_{t\to\infty} e = 0$, $\lim_{t\to\infty} \tilde{\xi} = 0$, $\lim_{t\to\infty} \tilde{f}_h = 0$, $\lim_{t\to\infty} \tilde{K}_{hp} = 0$, $\lim_{t\to\infty} \tilde{K}_{hd} = 0$, $\lim_{t\to\infty} \tilde{W}_h = 0$, and $\lim_{t\to\infty} x = x_h$.

Case 2: If $\dot{V} \geq 0$, it leads to

$$\begin{aligned} & \dot{e}^T K_d \dot{e} + \tilde{\xi}^T (L-A)\tilde{\xi} + \alpha \hat{u}_h^T \hat{u}_h + \dot{x}^T K_{hd} \dot{x} \\ = \;& \lambda_d \|\dot{e}\|^2 + \lambda_L \|\tilde{\xi}\|^2 + \alpha \|\hat{u}_h\|^2 + \lambda_{hd} \|\dot{x}\|^2 \\ \leq \;& -\dot{x}^T W_h \phi - \dot{x}^T \varepsilon + \varepsilon^T B^T \tilde{\xi} + \alpha \varepsilon^T \hat{u}_h \\ \leq \;& \frac{1}{2}(\|\dot{x}\|^2 + \|W_h\|^2) + \frac{1}{2}(\|\dot{x}\|^2 + \|\varepsilon\|^2) \\ & + \frac{1}{2}(\|\varepsilon\|^2 + \|B\|^2 \|\tilde{\xi}\|^2) + \frac{\alpha}{2}(\|\varepsilon\|^2 + \|\hat{u}_h\|^2) \\ \leq \;& \frac{1}{2}(\|\dot{x}\|^2 + b_W^2) + \frac{1}{2}(\|\dot{x}\|^2 + \varepsilon_B^2) + \frac{1}{2}(\varepsilon_B^2 + b_B^2 \|\tilde{\xi}\|^2) \\ & + \frac{\alpha}{2}(\varepsilon_B^2 + \|\hat{u}_h\|^2) \end{aligned} \tag{26}$$

where $\|\cdot\|$ stands for 2-norm of a matrix/vector, λ_d, λ_L and λ_{hd} are the minimal eigenvalues of K_d, $L-A$ and K_{hd}, respectively, b_W is the upper bound of W_h, b_B is the upper bound of B which is bounded according to Property 1, and ε_B is the upper bound of ε. By rearranging Eq. (26), we obtain

$$\begin{aligned} & \lambda_d \|\dot{e}\|^2 + (\lambda_L - \frac{b_B^2}{2})\|\tilde{\xi}\|^2 + \frac{\alpha}{2}\|\hat{u}_h\|^2 + (\lambda_{hd} - 1)\|\dot{x}\|^2 \\ & \leq \frac{b_W^2}{2} + \frac{\alpha + 2}{2}\varepsilon_B^2 \end{aligned} \tag{27}$$

Therefore, $\|\dot{e}\|$, $\|\tilde{\xi}\|$, $\|\hat{u}_h\|$ and $\|\dot{x}\|$ are bounded if

$$\lambda_d > 0,\ \lambda_L > \frac{b_B^2}{2},\ \alpha > 0 \ \text{ and } \lambda_{hd} > 1 \tag{28}$$

Furthermore, by choosing large K_d, L and α and having a large number of approximation nodes so that ε_B becomes sufficiently small, $\|\dot{e}\|$, $\|\tilde{\xi}\|$ and $\|\hat{u}_h\|$ can be made sufficiently small. For convenience of analysis, in the following we loosely state $\|\dot{e}\| \approx 0$, $\|\tilde{\xi}\| \approx 0$ and $\|\hat{u}_h\| \approx 0$ when $t \to \infty$, indicating that they become small enough when $t \to \infty$.

Suppose $\lim_{t\to\infty} \dot{\tilde{\xi}}$ exists, $\|\tilde{\xi}\| \approx 0$ leads to $\|\dot{\tilde{\xi}}\| \approx 0$. Therefore, according to Eq. (13), we have $\|\tilde{u}_h\| \approx 0$ and thus $\|u_h\| \approx 0$ since $\|\hat{u}_h\| \approx 0$. Note that $\|\tilde{u}_h\| \approx 0$ does not necessarily yield $\tilde{f}_h \approx 0$, $\tilde{K}_{hp} \approx 0$, $\tilde{K}_{hd} \approx 0$ and $\tilde{W}_h \approx 0$. To obtain $\tilde{f}_h \approx 0$, $\tilde{K}_{hp} \approx 0$, $\tilde{K}_{hd} \approx 0$ and $\tilde{W}_h \approx 0$, the signal $[1\ x^T\ \dot{x}^T\ \phi^T]$ needs to meet the persistent excitation (PE) requirement. In specific, according to Eq. (15), $\|\tilde{u}_h\| \approx 0$ yields

$$-\tilde{f}_h - \tilde{K}_{hp} x - \tilde{K}_{hd} \dot{x} - \tilde{W}_h \phi(x, \dot{x}) \approx 0 \tag{29}$$

by considering $\varepsilon \approx 0$. Rearranging Eq. (29), we have

$$[\tilde{f}_{h,i}\ \tilde{K}_{hp,i}\ \tilde{K}_{hd,i}\ \tilde{W}_{h,i}][1\ x^T\ \dot{x}^T\ \phi^T]^T \approx 0 \tag{30}$$

where $\tilde{f}_{h,i}$ stands for the i-th element of f_h, and $\tilde{K}_{hp,i}$, $\tilde{K}_{hd,i}$ and $\tilde{W}_{h,i}$ the i-th rows of $\tilde{K}_{hp}$, $\tilde{K}_{hd}$ and $\tilde{W}_h$, respectively. From Eq. (30), $[\tilde{f}_{h,i}\ \tilde{K}_{hp,i}\ \tilde{K}_{hd,i}\ \tilde{W}_{h,i}] \approx 0$ if the pseudo inverse of $[1\ x^T\ \dot{x}^T\ \phi^T]$ exists.

Considering $\|u_h\| \approx 0$, $\|\dot{e}\| \approx 0$ and the closed-loop dynamics (9), we have $\|e\| \approx 0$. According to Assumption 1, $u_h \approx 0$ also indicates that $K_{hp} \approx 0$ or $x \approx x_h$ if K_{hp} is nonzero.

The following theorem summarizes the results of the above two cases.

Theorem 2: Consider the system dynamics in Eq. (1), the human's and robot's respective controllers (2) and (6). By designing the observer Eq. (11) with the update laws (20) and updating the robot's reference trajectory according to Eq. (23), we achieve that

- $\lim_{t\to\infty} e \approx 0$ which indicates that the robot's actual trajectory x tracks its reference trajectory x_r.
- $\lim_{t\to\infty} x \approx x_h$ which indicates that the robot's actual trajectory x reaches the human's target position x_h.
- $\lim_{t\to\infty} \tilde{u}_h \approx 0$ which indicates that the estimation of the human's control input is achieved.

if K_d, L and α are chosen to be large and ε_B to be made small and if they satisfy

$$\lambda_d > 0, \lambda_L > \frac{b_B^2}{2}, \alpha > 0, \lambda_{hd} > 1 \tag{31}$$

where λ_d, λ_L and λ_{hd} are minimal eigenvalues of K_d, $L-A$ and K_{hd}, respectively, and b_B is the upper bound of B.

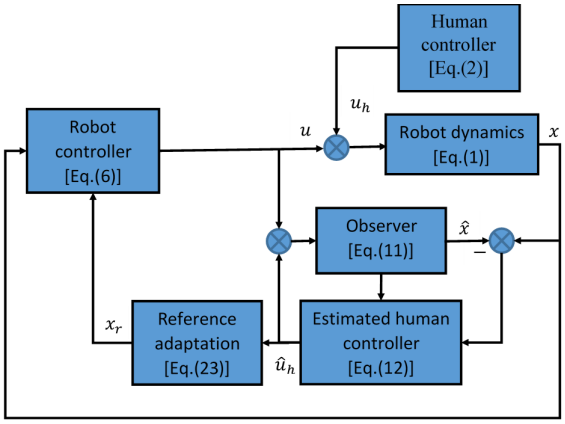

Fig. 1: Block diagram of our proposed control framework

C. Remarks

For the purpose of implementation, our proposed control method is depicted in Fig. 1. In this section, it will be interpreted by comparing with sensorless force control and impedance control.

Force estimation has been investigated in the field of robot control and many existing works use observers, e.g., [37], [38]. In our proposed framework, we use the estimated human input to adapt the robot's reference trajectory in (23) to track the human's unknown motion intention x_h, which was not considered in the literature. In fact, existing works on force estimation can be combined with our proposed motion intention estimation method.

Our proposed method also relates to impedance control in the sense that the interaction force is modulated by refining the robot's reference trajectory. However, impedance control

generates a virtual reference trajectory but its real reference trajectory does not change. Under impedance control with zero stiffness, the robot becomes a system passively responding to the human. In comparison, the proposed method updates the robot's reference trajectory and enables the robot to proactively move to the human's target position thus reducing the human's effort. As a matter of fact, our proposed motion intention estimation method can be combined with impedance control as explained in the following.

Herein we carry out mathematical analysis of a simplified case to compare existing methods (sensorless force control and impedance control) and the proposed one. Let us first consider impedance control with the following impedance model:

$$M\ddot{x} + D\dot{x} = \hat{u}_h \tag{32}$$

where M and D are desired inertia and damping matrices. We then consider a simplified version of the human controller in Eq. (2), by ignoring the damping gain and uncertainty:

$$u_h = -K_h(x - x_h) \tag{33}$$

where K_h is the stiffness gain in the simplified human controller. Suppose that the external force (or human control input) can be accurately estimated based on the sensorless force control method in [38], i.e. $\hat{u}_h = u_h$. Substituting Eq. (33) into Eq. (32) yields

$$M\ddot{x} + D\dot{x} + K_h x = K_h x_h \tag{34}$$

It is trivial to see that x will eventually converge to x_h. This explains how a zero-stiffness impedance controller with accurate force estimation can be used for human-driven robots.

By also using impedance control, the impedance model with the proposed method becomes

$$M\ddot{x} + D\dot{x} = \hat{u}_h - K_d(\dot{x} - \dot{x}_r) \tag{35}$$

where K_d is a positive definite matrix and the reference trajectory x_r is updated as in Eq. (23). Then, if $\hat{u}_h = u_h$, substituting (23) into (35) yields

$$M\ddot{x} + (D + K_d)\dot{x} + (\alpha K_d + 1)K_h = (\alpha K_d + 1)K_h x_h \tag{36}$$

By comparing with Eq. (34), Eq. (36) under the proposed method also guarantees the convergence of x to x_h. Moreover, the response with the proposed method is faster by simply checking the poles of two systems in Eqs. (34) and (36), if α is chosen properly. This indicates that the proposed method enables the robot to respond to the human more actively, which will be confirmed by the simulation results.

IV. Simulation

In this section, simulations are carried out to demonstrate the properties of our proposed observer and controller. A typical HRI scenario is considered: a 2-degrees-of-freedom (2-DoF) robot manipulator is driven by a human arm to manipulate an object in a planar task. The target position in the human controller is a fixed position point so the human's intended motion is a point-to-point movement. In an ideal situation, the robot can estimate the human control input by the developed observer, then the reference trajectory of the robot's end-effector is updated accordingly to minimize this estimated human control input. Using this strategy, the robot arm is expected to proactively move to the human's target position so that the human's control effort can be reduced. This advantage will be illustrated by comparing with impedance control with zero stiffness, as discussed in Section III.C.

A. Settings

For the convenience, we use m_i, l_i, l_{ci} and I_i to denote the physical parameters of the robot's link i: mass, link length, distance from the previous joint to the mass center and moment of inertia about the z-axis, respectively. According to [39], their values are set as in Table I.

TABLE I: Robot's physical parameters

Link	$m_i(kg)$	$l_i(m)$	$l_{ci}(m)$	$I_i(kgm^2)$
1	4.31871	0.3743	0.18715	0.000544
2	2.15197	0.2295	0.11475	0.000189

We set the robot arm's initial position as $x(0) = [0.2, 0.25]^T m$ and the human's target position as $x_h = [0.3, 0.35]^T m$. The control parameters in Eqs. (5) and (8) are selected as $K_{hp} = 50\,\mathbf{I}_2$, $K_{hd} = 10\,\mathbf{I}_2$, $\triangle = [\dot{x}_1^2, \dot{x}_2^2]^T$, $K_p = 180\,\mathbf{I}_2$, $K_d = 50\,\mathbf{I}_2$ where $\mathbf{I}_2$ represents a 2×2 unit matrix, RBFNN nodes number $l = 10$ and the observer parameters in Eq. (20) as $\alpha = 1.5$ and $L = [5, 1, 1, 0; 1, 4, 1, 1; 0.5, 0, 4, 0; 0, 2, 0, 5]$.

B. Results

Figs. 2 and 3 show the results of the robot arm's actual trajectory and reference trajectory along the x and y axes, respectively. We find that the human's target position x_h is accurately estimated by the robot and it is eventually reached by the robot. Fig. 4 shows that the NN weights $\hat{W}_h$ can converge to constant values, which are used to deal with uncertainties in the human model.

These simulation results demonstrate the validity of our proposed method in estimating the human partner's target position and in tracking of the updated robot's reference trajectory.

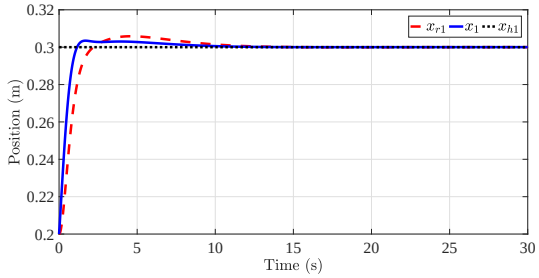

Fig. 2: Human's target position (x_{h1}), robot arm's reference trajectory (x_{r1}) and actual trajectory (x_1) along the x axis

In order to show the effect of RBFNN on the control performance, the simulation results with and without RBFNN are compared. The uncertainty component in the human input is set as $\Delta = \dot{x}^2 + (x - x_h)\sin(x - x_h)$, and the estimation without RBFNN is given as $\hat{u}_h = -\hat{f}_h - \hat{K}_{hp}x - \hat{K}_{hd}\dot{x}$ compared to Eq.

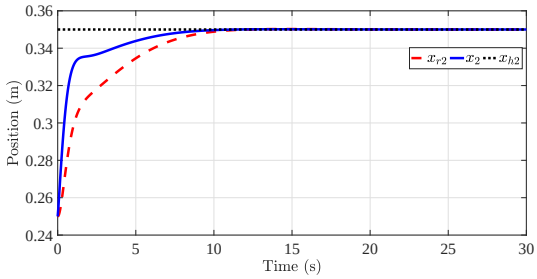

Fig. 3: Human's target position (x_{h2}), robot arm's reference trajectory (x_{r2}) and actual trajectory (x_2) along the y axis

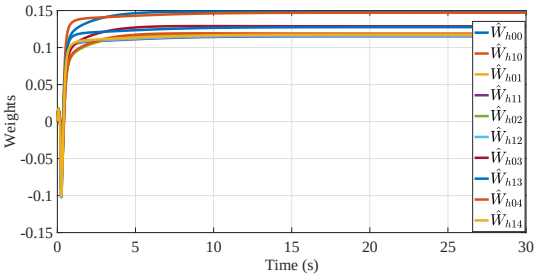

Fig. 4: Estimated weights of the neural networks. The first digit in the subscript of $\hat{W}_h$ corresponds to the argument of ϕ in Eq. (3), i.e. $Z = [x^T,\ \dot{x}^T]^T$: 1 represents the weight of $\dot{x}$ and 2 represents the weight of x. The second digit is the number of the NN nodes (the total number of nodes in the simulations is 10 and the weights for the first five nodes are shown due to limited space in the figure.

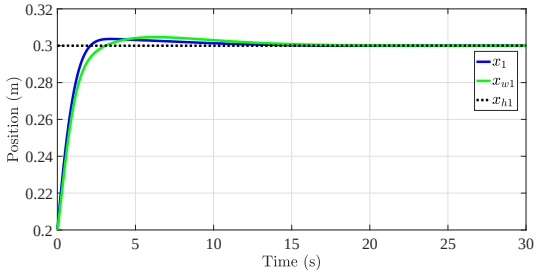

Fig. 5: Human's target position (x_{h1}), robot arm's actual trajectory with RBFNN (x_1) and without (x_{w1}) along the x axis.

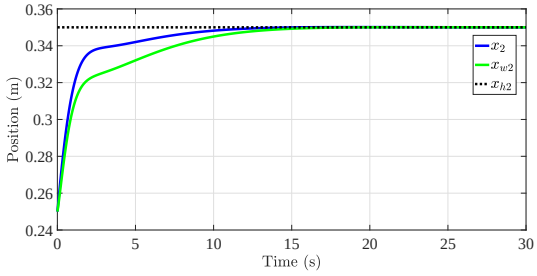

Fig. 6: Human's target position (x_{h2}), robot arm's actual trajectory with RBFNN (x_2) and without (x_{w2}) along the y axis.

(12). Results in Figs. 5 and 6 illustrate that the introduction of RBFNN improves the response speed, especially along the y axis.

C. Comparison with impedance control

In this section, we conduct a simulation to compare the proposed method with existing impedance control as explained in Section III-C. The following parameters are used: $M = 5$, $D = 10$, $K_h = 10$, $K_d = 10$, $\alpha = 1$, $x_h = \sin(t)$. The simulation results are shown in Fig. 7. The upper figure shows that the human force is much smaller with the proposed method, indicating reduced human control effort. The below figure shows that while the human's desired position 0.3m can be achieved by both methods, the system response with the proposed method is faster.

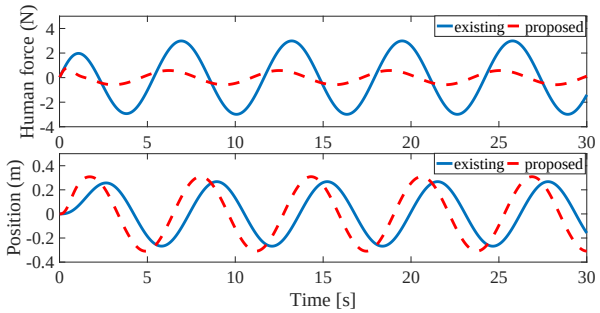

Fig. 7: Comparison between impedance control and the proposed method: human force (upper) and robot's position (below)

V. Experiment

In this section, the validity of our proposed method is further verified by experiments with a robotic platform Baxter, which has been developed by Rethink Robotics [40] (see Fig. 8).

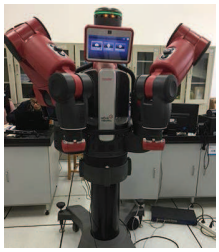

Fig. 8: Experiment platform

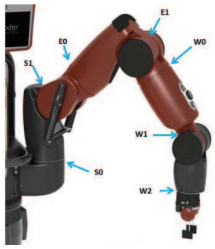

Fig. 9: Robotic joints

In this experiment, as shown in Fig. 9, we use two joints E1 and W1 of the Baxter's right arm so that its movement in the Cartesian space is in a plane. We decide not to use more than two joints for easier illustration of our proposed method. Position and velocity data are collected by the Baxter's controller, while the collected data are processed and our proposed method is implemented in a laptop with a 2-GHz Intel Core Processor. The laptop communicates with a computer dedicated to the Baxter via Ethernet in a frequency of 100Mb/s.

The parameters used in the experiment are the same as those in the simulation. In each control cycle, the laptop

retrieves the joint angle, estimates the human's target position, and sends the reference angle to Baxter. The control cycle in the experiment depends on the speed at which Baxter receives control data and returns joint position data, and its average value is about 1ms. Although Baxter is a robot which features passive compliance, we do not use this feature in the experiment. Instead, Baxter's inner position control loop is adopted, which raises an issue for the controller design since Baxter's control parameters are unknown. To address it, we choose L to be large enough so that $A-L$ becomes negative definite and thus the estimation error converges to zero. On the other hand, L cannot be too large otherwise too fast estimation will lead to a large overshoot and even instability.

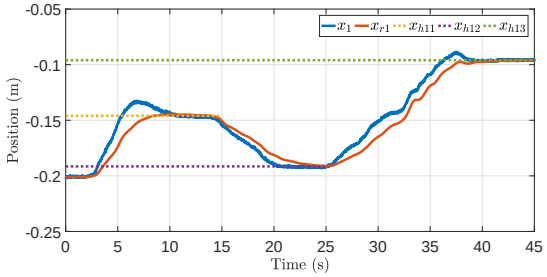

Fig. 10: Human's three target positions (x_{h11}, x_{h12}, x_{h13}), robot's reference trajectory (x_{r1}) and actual trajectory (x_1) along the x axis

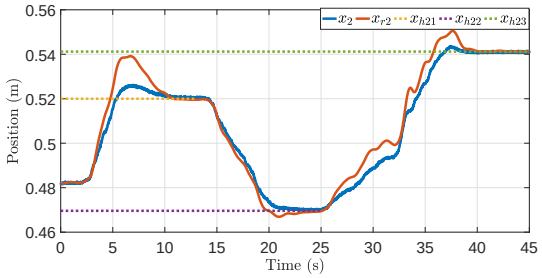

Fig. 11: Human's three target positions (x_{h21}, x_{h22}, x_{h23}), robot's reference trajectory (x_{r2}) and actual trajectory (x_2) along the y axis

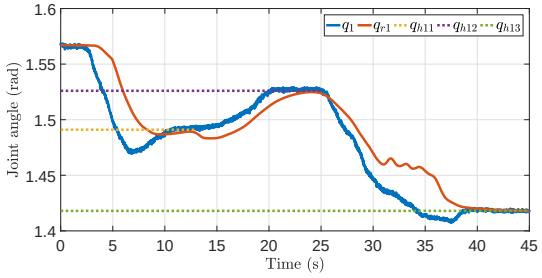

Fig. 12: Human's three target angles (q_{h11}, q_{h12}, q_{h13}), robot's reference angle (q_{r1}) and actual angle (q_1) of the first joint

During the experiment, the human moves the robot arm to his three target positions in the Cartesian space that are unknown to the robot. When the human stops exerting a force to the robot arm, it remains in its current position. Figs. 10 and 11 show the experimental results of the robot arm positions

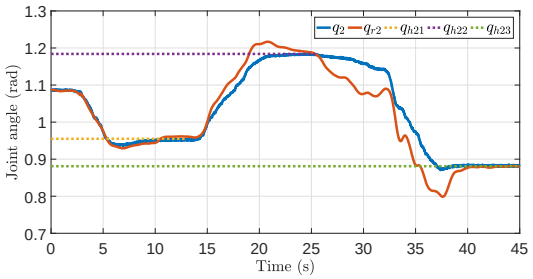

Fig. 13: Human's three target angles (q_{h21}, q_{h22}, q_{h23}), robot's reference angle (q_{r2}) and actual angle (q_2) of the second joint

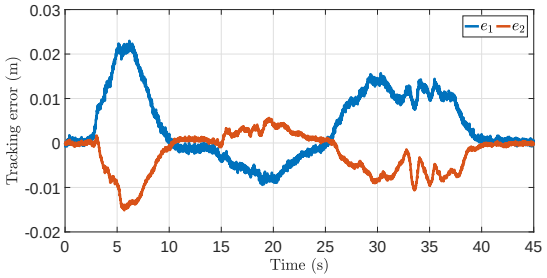

Fig. 14: Robot's tracking errors along the x axis (e_1) and y axis (e_2)

along two axes, illustrating that the human can lead the robot arm to his target positions. Moreover, the developed observer can accurately estimate the human's target positions. After reaching the last target position, the human remains in contact with the robot for a certain time to verify whether the tracking error can completely converge. Figs. 12 and 13 show how the robot arm's movement in the Cartesian space is realized by tracking of reference angles in the joint space. Fig. 14 illustrates that the tracking errors along axis x and axis y are within an acceptable range.

Corresponding to these results, snapshots of the experimental process are shown in Fig. 15. In these figures, we have used the white lines to mark the robot arm's initial position so its movement revolution can be clearly seen. These figures illustrate that the robot arm moves according to the intention of its human partner, whose three target positions are reached in sequence.

VI. Conclusions

The presented experiment has demonstrated the features of the designed controller in a simple scenario of human-

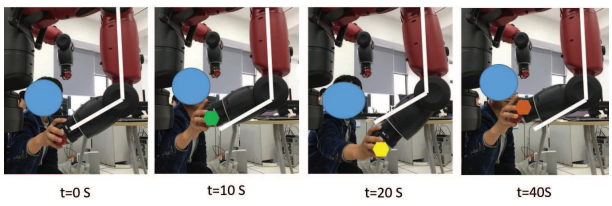

Fig. 15: Snapshots of the experimental process. The initial configuration of the robot arm is shown by a white line, the human's three target positions are marked by three hexagons with different colors, and a blue circle is used to cover the face of the human.

driven robots, where the human guided the robot to his target positions through direct physical contact. This experiment was carried out without considering an object manipulated by the human and robot and it was assumed that the object could be an extension of the robot arm if there is no relative motion between them. In a real-world application, e.g. luggage loading and offloading in airports, the relative motion between the robot, object and human arm may have significant effects on the manipulation performance, so this issue needs to be investigated in our future works.

This paper only shows the feasibility of the proposed method with 2-DoFs of the robot arm, while in theory it can be applied to a robot with more DoFs. In the later case, the coupling effects of different directions and redundancy problem may need to be addressed when implementing the proposed method. While our proposed method is discussed and implemented in the Cartesian space, it can be also applied to the joint space. This is useful in applications such as robotic exoskeleton, where it needs to detect the human user's motion intention in its joint space and moves its own joints correspondingly [41]. This will be investigated and tested on a lower-limb exoskeleton that has been developed in one of our previous works [42].

HRI has been studied to testify the usefulness of the observer developed in this paper. As a matter of fact, this observer can also estimate the contact force exerted by a passive environment. For example, our proposed method may be useful in haptic exploration or surface polishing, where the contact force needs to be regulated. This possibility will be explored in the future works.

APPENDIX

A. Proof of Theorem 1

Substituting human's and robot's respective controllers (2) and (6) into the system dynamics in Eq. (1), and considering the conditions stated in Theorem 1, we can obtain the following error dynamics

$$M_x(q)\,\ddot{e} + (C_x(q,\dot{q}) + K_d + K_{hd})\,\dot{e} + (K_p + K_{hp})e = 0 \qquad (37)$$

where

$$e = x - x_r = x - x_h \qquad (38)$$

Now, let us consider a Lyapunov function candidate

$$W = \frac{1}{2}(\dot{e}^T M_x \dot{e} + e^T (K_p + K_{hp})e) \qquad (39)$$

Taking the time derivative of W, we can obtain

$$\dot{W} = \dot{e}^T (M_x \ddot{e} + \frac{1}{2}\dot{M}_x \dot{e}) + \dot{e}^T (K_p + K_{hp})e \qquad (40)$$

Considering Property 2 and the error dynamics in Eq. (37), we can obtain

$$\begin{aligned} \dot{W} &= \dot{e}^T (M_x \ddot{e} + C_x \dot{e} + (K_p + K_{hp})e) \\ &= \dot{e}^T (-(K_d + K_{hd})\dot{e}) \\ &= -\dot{e}^T (K_d + K_{hd})\dot{e} \end{aligned} \qquad (41)$$

Therefore, $\dot{W}$ is non-positive since K_d is designed to be positive definite and K_{hd} assumed to be positive definite. Next, the following two cases of $\dot{W}$ will be discussed.

Case 1 $\dot{W} < 0$ indicates that W moronically decreases. Since $W \geq 0$, it yeilds that $\lim_{t\to\infty} W = 0$. According to the definition of W, we can obtain $\lim_{t\to\infty} \dot{e} = 0$ and $\lim_{t\to\infty} e = 0$.

Case 2 If $\dot{W} = 0$, then $\dot{e} = 0$ which leads to $e = 0$ by considering the closed-loop dynamics (37).

In both cases, $\lim_{t\to\infty} e = 0$ and this completes the proof.

REFERENCES

[1] C. Passenberg, N. Stefanov, A. Peer, and M. Buss, "Enhancing task classification in human-machine collaborative teleoperation systems by real-time evaluation of an agreement criterion," in *IEEE World Haptics Conference*, (Istanbul, Turkey), pp. 493–498, 2011.

[2] C. Yang, H. Wu, Z. Li, W. He, N. Wang, and C. Su, "Mind control of a robotic arm with visual fusion technology," *IEEE Transactions on Industrial Informatics*, vol. 14, no. 9, pp. 3822–3830, 2018.

[3] Z. Li, B. Huang, A. Ajoudani, C. Yang, C. Y. Su, and A. Bicchi, "Asymmetric bimanual control of dual-arm exoskeletons for human-cooperative manipulations," *IEEE Transactions on Robotics*, vol. 34, no. 1, pp. 264–271, 2018.

[4] Y. Hu, M. Benallegue, G. Venture, and E. Yoshida, "Interact with me: An exploratory study on interaction factors for active physical human-robot interaction," *IEEE Robotics and Automation Letters*, vol. 5, no. 4, pp. 6764–6771, 2020.

[5] K. Kronander and A. Billard, "Stability considerations for variable impedance control," *IEEE Transactions on Robotics*, vol. 32, no. 5, pp. 1298–1305, 2016.

[6] F. Dimeas and N. Aspragathos, "Online stability in human-robot cooperation with admittance control," *IEEE Transactions on Haptics*, vol. 9, no. 2, pp. 267–278, 2016.

[7] H. Cai and Y. Mostofi, "A human-robot collaborative traveling salesman problem: Robotic site inspection with human assistance," in *2016 American Control Conference (ACC)*, (Boston, MA, USA), pp. 6170–6176, 2016.

[8] H. Liu and L. Wang, "Human motion prediction for human-robot collaboration," *Journal of Manufacturing Systems*, vol. 44, no. 2, pp. 287–294, 2017.

[9] Q. Gao, J. Liu, Z. Ju, and X. Zhang, "Dual-hand detection for humancrobot interaction by a parallel network based on hand detection and body pose estimation," *IEEE Transactions on Industrial Electronics*, vol. 66, no. 12, pp. 9663–9672, 2019.

[10] Y. Li and C. Yang, *A Hybrid Human Motion Prediction Approach for Human-Robot Collaboration*. Advances in Computational Intelligence Systems, vol. 1043, Springer, Cham, 2020.

[11] M. Khatib, K. A. Khudir, and A. D. Luca, "Human-robot contactless collaboration with mixed reality interface," *Robotics and Computer-Integrated Manufacturing*, vol. 67, no. 1, pp. 1–12, 2020.

[12] P. Gustavsson, A. Syberfeldt, R. Brewster, and L. Wang, "Human-robot collaboration demonstrator combining speech recognition and haptic control," *Procedia CIRP*, vol. 63, no. 1, pp. 396–401, 2017.

[13] H. Liu and L. Wang, "Gesture recognition for human-robot collaboration: A review," *International Journal of Industrial Ergonomics*, vol. 68, no. 1, pp. 355–367, 2017.

[14] D. Feth, "Haptic human-robot collaboration: Comparison of robot partner implementations in terms of human-likeness and task performance," *Presence*, vol. 20, no. 2, pp. 173–189, 2011.

[15] Y. Maeda, H. Takayuki, and A. Tamio, "Human-robot cooperative manipulation with motion estimation," in *Proceedings of IEEE/RSJ International Conference on Intelligent Robots and Systems*, (Maui, HI, USA), pp. 2240–2245, 2001.

[16] Z. Wang, A. Peer, and M. Buss, "An HMM approach to realistic haptic human-robot interaction," in *Proceedings of World Haptics - Third Joint Eurohaptics Conference*, (Salt Lake City, UT, USA), pp. 374–379, 2009.

[17] Y. Li and S. S. Ge, "Force tracking control for motion synchronization in human-robot collaboration," *Robotica*, vol. 34, no. 6, pp. 1260–1281, 2016.

[18] V. Duchaine and C. M. Gosselin, "General model of human-robot cooperation using a novel velocity based variable impedance control," in *Proceedings of World Haptics-Second Joint EuroHaptics Conference*, (Tsukuba, Japan), pp. 446–451, 2007.

[19] S. Cremer, S. K. Das, I. B. Wijayasinghe, D. O. Popa, and F. L. Lewis, "Model-free online neuroadaptive controller with intent estimation for physical human-robot interaction," *IEEE Transactions on Robotics*, vol. 36, no. 1, pp. 240–253, 2020.

[20] W. Zhao, L. Sun, C. Liu, and M. Tomizuka, "Experimental evaluation of human motion prediction toward safe and efficient human robot collaboration," in *2020 American Control Conference (ACC)*, (Denver, CO, USA), pp. 4349–4354, 2020.

[21] M. S. Erden and T. Tomiyama, "Human-intent detection and physically interactive control of a robot without force sensors," *IEEE Transactions on Robotics*, vol. 26, no. 2, pp. 370–382, 2010.

[22] W. Sheng, A. Thobbi, and Y. Gu, "An integrated framework for human-robot collaborative manipulation," *IEEE Transactions on Cybernetics*, vol. 45, no. 10, pp. 2030–2041, 2015.

[23] N. Hogan, "Impedance control: an approach to manipulation-Part I: Theory; Part II: Implementation; Part III: Applications," *Journal of Dynamic Systems, Measurement, and Control*, vol. 107, no. 1, pp. 1–24, 1985.

[24] L. Yang, Y. Li, and D. Huang, "Motion synchronization in human-robot co-transport without force sensing," in *2018 37th Chinese Control Conference (CCC)*, (Wuhan, China), pp. 5369–5374, 2018.

[25] J. Craig, *Adaptive Control of Mechanical Manipulators*, vol. Reading, MA:. Addison-Welsley, 1988.

[26] E. Burdet, D. W. Franklin, and T. E. Milner, *Human Robotics - Neuromechanics and Motor Control*. MIT Press, 2013.

[27] M. Rahman, R. Ikeura, and K. Mizutani, "Investigation of the impedance characteristic of human arm for development of robots to cooperate with humans," *JSME International Journal Series C*, vol. 45, no. 2, pp. 510–518, 2002.

[28] Y. Li and S. S. Ge, "Human-robot collaboration based on motion intention estimation," *IEEE/ASME Transactions on Mechatronics*, vol. 19, no. 3, pp. 1007–1014, 2014.

[29] E. J. Perreault, R. F. Kirsch, and P. E. Crago, "Multijoint dynamics and postural stability of the human arm.," *Experimental Brain Research*, vol. 157, no. 4, pp. 507–517, 2004.

[30] F. A. Mussa-Ivaldi, N. Hogan, and E. Bizzi, "Neural, mechanical, and geometric factors subserving arm posture in humans," *The Journal of Neuroscience*, vol. 5, no. 10, pp. 2732–2743, 1985.

[31] P. Stalph, *Analysis and Design of Machine Learning Techniques*. Springer, 2014.

[32] W. He, H. Huang, and S. S. Ge, "Adaptive neural network control of a robotic manipulator with time-varying output constraints," *IEEE Transactions on Cybernetics*, vol. 47, no. 10, pp. 3136–3147, 2017.

[33] R. M. Sanner and J. E. Slotine, "Gaussian networks for direct adaptive control," *IEEE Transactions on Neural Networks*, vol. 3, no. 6, pp. 837–863, 1992.

[34] "Zero-order hold." [Online]. https://en.wikipedia.org/wiki/Zero-orderhold.

[35] E. W. Weisstein, "Piecewise constant function." From MathWorld–A Wolfram Web Resource. https://mathworld.wolfram.com/PiecewiseConstantFunction.html.

[36] E. Burdet, R. Osu, D. W. Franklin, T. E. Milner, and M. Kawato, "The central nervous system stabilizes unstable dynamics by learning optimal impedance," *Nature*, vol. 414, p. 446C449, 2001.

[37] N. Vitiello, T. Lenzi, S. M. M. D. Rossi, S. Roccella, and M. C. Carrozza, "A sensorless torque control for antagonistic driven compliant joints," *Mechatronics*, vol. 20, no. 3, pp. 355–367, 2010.

[38] M. Capurso, M. M. G. Ardakani, R. Johansson, A. Robertsson, and P. Rocco, "Sensorless kinesthetic teaching of robotic manipulators assisted by observer-based force control," in *2017 IEEE International Conference on Robotics and Automation (ICRA)*, (Singapore), pp. 945–950, 2017.

[39] C. Fitzgerald, "Developing Baxter," in *2013 IEEE International Conference on Technologies for Practical Robot Applications*, (Woburn, Massachusetts, USA.), pp. 1–6, 2013.

[40] A. Smith, C. Yang, and C. Li, "Development of a dynamics model for the Baxter robot," in *2016 IEEE International Conference on Mechatronics and Automation*, (Harbin, China), pp. 1244–1249, 2016.

[41] Z. Li, B. Huang, Z. Ye, M. Deng, and C. Yang, "Physical human-robot interaction of a robotic exoskeleton by admittance control," *IEEE Transactions on Industrial Electronics*, vol. 65, no. 12, pp. 9614–9624, 2018.

[42] Y. Yang, L. Ma, and D. Huang, "Development and repetitive learning control of lower limb exoskeleton driven by electrohydraulic actuators," *IEEE Transactions on Industrial Electronics*, vol. 64, no. 5, pp. 4169–4178, 2017.

Yanan Li (M'14-SM'21) received the B.Eng. and M.Eng. degrees from the Harbin Institute of Technology, China, in 2006 and 2008, respectively, and the PhD degree from the National University of Singapore, in 2013. Currently he is a Senior Lecturer in Control Engineering with the Department of Engineering and Design, University of Sussex, UK. From 2015 to 2017, he has been a Research Associate with the Department of Bioengineering, Imperial College London, UK. From 2013 to 2015, he has been a Research Scientist with the Institute for Infocomm Research (I2R), Agency for Science, Technology and Research (A*STAR), Singapore. His general research interests include human-robot interaction, assistive robotics, human motor control and control theory and applications.

Lin Yang received the B.Eng. degree of automation from the Sichuan University of Science and Engineering, China, in 2017, the M.Eng. degree in Control Engineering at the School of Electrical Engineering, Southwest Jiaotong University, Chengdu, China, in 2020. His general research interests include physical human-robot collaboration and machine learning.

Deqing Huang (M'10-SM'19) received the B.S. and Ph.D. degrees in applied mathematics from the Mathematical College, Sichuan University, Chengdu, China, in 2002 and 2007, respectively, and the Ph.D. degree in control engineering from the National University of Singapore (NUS), Singapore, in 2011. From 2013 to 2016, he was a Research Associate with the Department of Aeronautics, Imperial College London, London, U.K. In 2016, he joined the Department of Electronic and Information Engineering, Southwest Jiaotong University, Chengdu, as a Professor and the Department Head. His current research interests include modern control theory, fluid analysis and control, convex optimization, and robotics.

Chenguang Yang (M'10-SM'16) received the Ph.D. degree in control engineering from the National University of Singapore, Singapore, in 2010, and postdoctoral training in human robotics from the Imperial College London, London, U.K. He was awarded UK EPSRC UKRI Innovation Fellowship and individual EU Marie Curie International Incoming Fellowship. As the lead author, he won the IEEE Transactions on Robotics Best Paper Award (2012) and IEEE Transactions on Neural Networks and Learning Systems Outstanding Paper Award (2022) .He is a Co-Chair of IEEE Technical Committee on Collaborative Automation for Flexible Manufacturing (CAFM) and a Co-Chair of IEEE Technical Committee on Bio-mechatronics and Bio-robotics Systems (B2S). He serves as Associate Editors of a number of international top journals including Neurocomputing and seven IEEE Transactions. His research interest lies in human robot interaction and intelligent system design.

Jingkang Xia received the B.Eng. degree in electrical information and engineering, from the School of Electrical Engineering, Southwest Minzu University, Chengdu, China, in 2018. He is currently pursuing the Ph.D. degree in control theory and application with the School of Electrical Engineering, Southwest Jiaotong University, Chengdu, China. His current research interests include human-robot collaboration, robotics and intelligent control systems.